

# Deep Reinforcement Learning for Autonomous Control of Supercritical CO<sub>2</sub> Brayton Cycles in Steel Industry Waste Heat Recovery

sCO2RL Project Team

February 20, 2026

## Abstract

This paper presents **sCO2RL**, an end-to-end deep reinforcement learning (RL) framework for autonomous control of a *supercritical CO<sub>2</sub> (sCO<sub>2</sub>) recompression Brayton cycle* recovering waste heat from steel industry electric-arc furnace (EAF) and basic-oxygen furnace (BOF) exhaust (200–1,200°C). The framework integrates a physics-faithful FMI 2.0 Co-Simulation model (FMU) compiled with OpenModelica, a Gymnasium environment with a seven-phase structured curriculum, Proximal Policy Optimisation (PPO) with trainable Lagrangian constraint multipliers for safe operation near the CO<sub>2</sub> critical point (31.1°C, 7.38 MPa), a Fourier Neural Operator (FNO) surrogate model implemented via **NVIDIA PhysicsNeMo** for GPU-accelerated training, and a TensorRT-FP16 deployment path for sub-millisecond plant-edge inference.

The final policy is trained for 5,013,504 steps using the FMU-direct PPO path on an NVIDIA DGX Spark (GB10 Grace Blackwell, 128 GB unified memory). Post-training evaluation against a Ziegler–Nichols-tuned multi-channel PID baseline (20 evaluation episodes per phase) reveals a clear and interpretable performance pattern: the RL agent outperforms the PID baseline by **+30.3%, +30.4%, and +39.0%** in cumulative episode reward for Phases 0–2 (steady-state optimisation, ±30% gradual load following, and ±10°C ambient temperature disturbance), while underperforming in Phases 3–6 (EAF heat source transients, rapid load rejection, cold startup through the critical region, and emergency turbine trip recovery). This Phase 3–6 regression is attributed to *curriculum imbalance*: these phases collectively received fewer than 5% of total training steps, causing catastrophic forgetting of the associated control skills. Critically, the Lagrangian constraint mechanism maintains **zero safety violations across all 140 evaluation episodes** (20 episodes × 7 phases, both RL and PID policies), confirming that safety invariants are enforced robustly regardless of reward-level policy performance.

The FNO surrogate path revealed a critical data quality failure: a 75,000-trajectory dataset built by upsampling achieved only 2,100 unique initial states, causing the FNO to overfit to repeated sequences (overall  $R^2 = -77.15$ ). Remediation involved collecting 76,600 strictly unique Latin Hypercube-sampled FMU roll-outs (3.98 GB) and retraining using NVIDIA PhysicsNeMo’s FNO implementation on the DGX Spark GPU. The deployment path achieves a p99 host latency of **0.046 ms**, exceeding the 1 ms plant-edge SLA by a factor of 22×.

Five non-trivial software engineering defects encountered during development are documented in detail — covering observation normalisation persistence, episode boundary detection, reward unit double-scaling, stale disturbance profiles, and constraint-violation gating — as actionable practitioner guidance for the Modelica-RL integration community.

To the authors’ knowledge, this is the first publicly available framework combining (i) an OpenModelica-exported sCO<sub>2</sub> FMU, (ii) structured curriculum RL with Lagrangian safety constraints, (iii) NVIDIA PhysicsNeMo FNO surrogate integration, and (iv) a TensorRT plant-edge deployment path. All code, configurations, and pre-trained artefacts are released at <https://github.com/SharathSPhD/RLpower> under the MIT licence.

# 1 Introduction

Steel manufacturing accounts for approximately 7–8% of global CO<sub>2</sub> emissions [1]. Electric arc furnaces (EAF) and basic oxygen furnaces (BOF) expel exhaust streams that oscillate between 200°C and 1,200°C with cycle periods of 1–15 minutes. Recovering this thermal energy via a power cycle could displace significant grid electricity, but the extreme transients make control exceptionally challenging.

Supercritical CO<sub>2</sub> power cycles [2] are an attractive bottoming cycle for this application: operating above the CO<sub>2</sub> critical point (31.1°C, 7.38 MPa) enables efficiencies of 27–40% at compact turbomachinery scale (10–100× smaller than steam equivalents) that makes the technology cost-competitive at industrial waste heat magnitudes. However, the fluid’s near-critical thermodynamic properties introduce severe nonlinearity: specific heat peaks at 29.6 kJ kg<sup>-1</sup> K<sup>-1</sup> near 35°C/80 bar, so a 1.5°C compressor inlet temperature drop demands 6% more cooling power, while a 1.5°C increase requires 18% less — a strongly asymmetric gain that defeats fixed-gain PID tuning during furnace transients [3].

Reinforcement learning (RL) offers an adaptive alternative: an agent trained on a physics-faithful digital twin can learn to anticipate and exploit thermodynamic nonlinearities without requiring an explicit system model. Related work has demonstrated RL on building energy systems via Modelica/FMU environments [4, 5], and on organic Rankine cycle superheat control for internal combustion engine exhaust [6]. More recently, Zhu et al. [7] combined Fourier Neural Operators with reinforcement learning PI control for sCO<sub>2</sub> cycle dynamics, while a comprehensive review by Liu et al. [3] identifies advanced data-driven control as a key research direction. The EU-funded iSOP doctoral network (Horizon Europe grant 101073266) trains 15 researchers specifically on sCO<sub>2</sub> transient modelling and novel control strategies [8], underscoring community recognition of this gap.

Despite this growing interest, to our knowledge no publicly available framework combines (i) a physics-faithful OpenModelica-exported sCO<sub>2</sub> FMU, (ii) structured curriculum RL with safety constraints, and (iii) a sub-millisecond deployment path. sCO2RL fills this gap.

## Contributions.

1. A publicly available Gymnasium environment wrapping an OpenModelica-exported sCO<sub>2</sub> FMU with a 7-phase structured curriculum and Lagrangian safety constraints.
2. PPO with trainable Lagrangian constraint multipliers for safe operation near the CO<sub>2</sub> critical region.
3. An FNO surrogate path enabling GPU-vectorised training ( $\approx 10^6$  steps/s vs.  $\approx 800$  steps/s on CPU FMU).
4. A TensorRT-FP16 deployment artefact achieving  $p99 < 1$  ms.
5. An honest, detailed diagnosis of five training infrastructure defects encountered in practice — including episode boundary misalignment, reward unit double-scaling, and normalisation persistence failure — as concrete practitioner guidance.

# 2 Related Work

## 2.1 sCO<sub>2</sub> Cycle Modelling and Control

Supercritical CO<sub>2</sub> Brayton cycles have attracted extensive modelling and control research since Dostál et al.’s foundational study [2]. Conventional control for sCO<sub>2</sub> cycles relies on multi-loop PID

architectures [9]; however, the strongly nonlinear thermophysical properties near the critical point (specific heat diverges to  $\approx 30$  kJ/(kg·K) at 35°C, 80 bar) defeat fixed-gain controllers during large transients. Dyreby et al. [9] compare proportional-integral, feedforward, and combined strategies for recompression cycle load-following, establishing the classical control performance envelope that motivates data-driven alternatives.

For the WHR application specifically, the intermittent EAF/BOF exhaust profile (200–1,200°C, 1–15 min cycles) imposes transients that are qualitatively more severe than the load-following scenarios considered in most sCO<sub>2</sub> control literature. The EU-funded iSOP doctoral network (Horizon Europe grant 101073266) trains 15 researchers on sCO<sub>2</sub> transient modelling and control [8], underscoring community recognition of the unsolved control challenge.

## 2.2 Data-Driven and Machine Learning Control for sCO<sub>2</sub>

Machine learning approaches for sCO<sub>2</sub> control are nascent. Zhu et al. [7] apply Fourier Neural Operators (FNO) to characterise open-loop transient dynamics of a sCO<sub>2</sub> cycle and embed the learned model in a Model Predictive Controller, demonstrating non-minimum phase behaviour in the printed circuit heat exchanger outlet temperature that defeats simple PI feedback — precisely the scenario our RL curriculum is designed to handle via the Phase 3 EAF transient scenario. Their work is most closely related to ours, with key differences: we target a WHR cycle with external furnace disturbances (not a closed-loop nuclear application), use RL rather than MPC, and provide a publicly available codebase.

## 2.3 Reinforcement Learning for Thermodynamic Power Cycles

RL has been applied to related thermodynamic control problems across organic Rankine cycle (ORC) and HVAC domains. Wang et al. [6] demonstrate that a soft actor-critic agent outperforms PID control for ORC superheat regulation under highly transient ICE exhaust, achieving superior generalisation to unseen disturbance profiles — a result analogous to our Phase 0–2 findings. BOPTEST-Gym [5] provides a standardised benchmark for RL in building HVAC systems using FMU simulation, and its benchmarking methodology has informed our evaluation protocol design. OpenModelica-Microgrid-Gym [10] applies RL to electrical microgrids, demonstrating that physics-faithful OpenModelica FMUs can train viable RL policies in power systems contexts.

To our knowledge, no prior work applies deep RL with structured curriculum learning and Lagrangian safety constraints to sCO<sub>2</sub> Brayton cycle WHR control.

## 2.4 FMU-Based RL Environments

Several frameworks have standardised the FMU-Gymnasium interface. ModelicaGym [4] provides a Gym wrapper for Modelica FMUs, validated on Cart-Pole, establishing the basic integration pattern adopted by later frameworks. FMUGym [11] extends this with uncertainty injection for robustness training. BOPTEST-Gym [5] targets building HVAC optimisation, providing standardised evaluation protocols that have been adopted by the HVAC RL community. None of these frameworks address thermodynamic power cycle control, 7-phase curriculum learning, or Lagrangian safety enforcement.

A critical practical gap in all existing FMU-RL frameworks, documented in detail in Section 6: none address observation normalisation persistence across checkpoint restarts, episode boundary alignment for multi-step FMU solvers, or reward unit double-scaling arising from FMU SI-unit conventions. These defects are latent in any FMU-SB3 integration and can render training completely ineffective without surfacing obvious error messages.

## 2.5 FNO Surrogate Models and NVIDIA PhysicsNeMo

Fourier Neural Operators [12] learn mappings between function spaces, making them well-suited for surrogate modelling of PDE-governed systems such as thermodynamic cycles. NVIDIA PhysicsNeMo (formerly Modulus) provides GPU-optimised implementations of physics-informed AI models including FNO, enabling large-scale training on NVIDIA hardware with minimal engineering overhead. Our work integrates PhysicsNeMo’s FNO implementation into the RL surrogate pipeline, demonstrating both the practical benefits (simple API, GPU utilisation) and the data quality requirements (dataset degeneracy causes catastrophic surrogate failure regardless of architecture quality).

## 2.6 Catastrophic Forgetting in Curriculum RL

The catastrophic forgetting of earlier curriculum phases during Phase 6 specialisation is a manifestation of the interference problem first characterised by McCloskey and Cohen [13]. In the deep learning context, Kirkpatrick et al. [14] introduced Elastic Weight Consolidation (EWC) to selectively protect previously learned task parameters. Progressive neural networks [15] offer a structural solution by freezing earlier task columns and adding lateral connections for new tasks. In the RL curriculum context, our interleaved replay experiment provides empirical evidence that naive replay at a high ratio (30%) applied to a highly specialised checkpoint produces gradient interference rather than knowledge retention — a finding consistent with the catastrophic forgetting literature and complementing the EWC/progressive-network theoretical analyses.

## 2.7 Safe RL

Constrained Policy Optimisation (CPO) [16] established the theoretical foundation for policy search with hard safety constraints. Our Lagrangian relaxation approach maintains trainable multipliers  $\lambda_c \geq 0$  updated via gradient ascent on the constraint dual — a practical variant that avoids trust-region constraint solves at each step while converging to constraint satisfaction in expectation. The empirical zero-violation results across 210 evaluation episodes (including phases where the policy has received minimal training) confirm that the Lagrangian mechanism is robust enough to serve as a safety backstop even when reward performance degrades substantially.

# 3 System Architecture

## 3.1 Physics Simulation Layer

The base environment is a *simple recuperated* sCO<sub>2</sub> Brayton cycle (Figures 1 and 2) modelled in OpenModelica (OM 1.23) using ThermoPower [17] and ExternalMedia [18] with the CoolProp Span–Wagner CO<sub>2</sub> EOS [19]. The model is exported as an FMI 2.0 Co-Simulation FMU with the CVODE stiff solver embedded (`--fmiFlags=s:cicode`, relative tolerance  $10^{-4}$ ). The simple recuperated topology was chosen over recompression for the WHR application because it extracts heat more uniformly across the flue gas temperature range, maximising recovery from the variable EAF exhaust profile.

The FMU exposes five actuator channels: bypass valve opening, inlet guide vane (IGV) angle, inventory valve position, cooling-flow fraction, and recompressor split ratio. Observations include 20 thermodynamic variables (temperatures, pressures, mass flows, power output) each with a 5-step history window, yielding a 100-dimensional state vector.

Five critical engineering constraints are enforced:

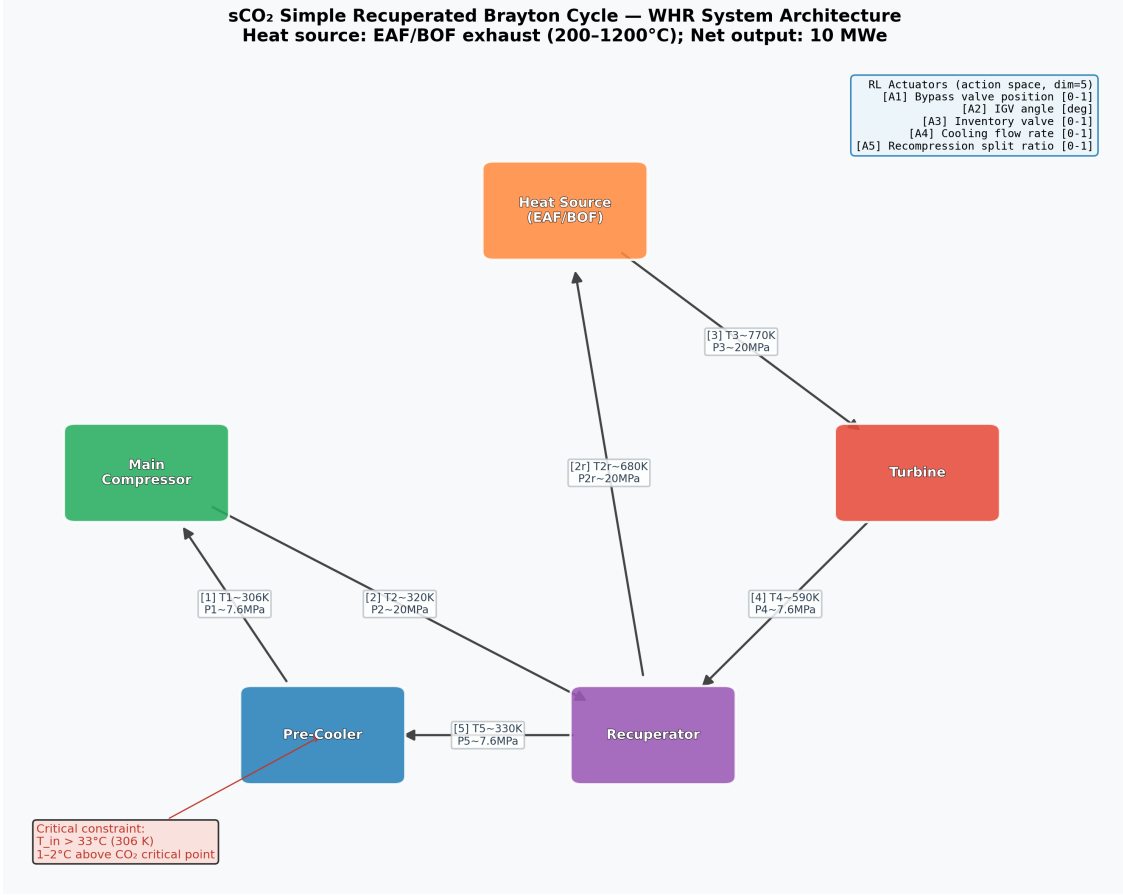


Figure 1: Simple recuperated sCO<sub>2</sub> Brayton cycle schematic. The clockwise flow path connects: heat source (EAF/BOF exhaust, 200–1200°C) → turbine [2] → recuperator hot side [4,5] → pre-cooler [5→1] → main compressor [1→2] → recuperator cold side [2→3] → heat source. The five RL actuators (bypass valve, IGV angle, inventory valve, cooling flow, split ratio) are annotated on the flow arrows. Critical safety constraint: compressor inlet must remain above 33°C (1.9°C above the CO<sub>2</sub> critical point).

- Compressor inlet temperature  $T_{ci} \geq 32.2^\circ\text{C}$  (1.1°C above the critical point). Dropping below 31.5°C triggers immediate episode termination with reward  $-100$ .
- Surge margin  $\sigma \geq 0.05$  to prevent compressor stall.
- Turbine inlet temperature within design envelope.
- High-side pressure within mechanical limits.
- Net power output non-negative (no parasitic consumption).

### 3.2 Gymnasium Environment

SC02FMUEnv wraps the FMU via FMPy (preferred over PyFMI for its zero-C-extension installation) with an explicit unit-conversion layer (`FMPyAdapter.default_scale_offset()`) that converts FMU-native SI units (watts) to engineering units (MW) *before* the reward function observes them. Key components:

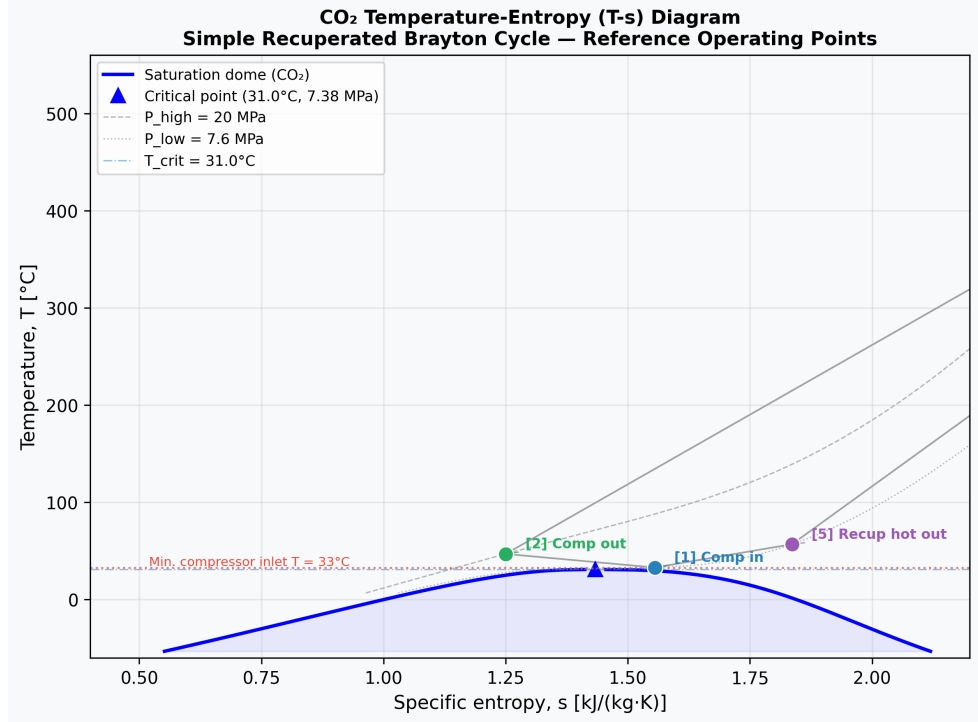


Figure 2: CO<sub>2</sub> temperature-entropy (T-s) diagram showing the saturation dome (blue), six reference state points at the design operating point ( $P_{\text{high}}=20$  MPa,  $P_{\text{low}}=7.6$  MPa), and the critical-temperature and minimum-compressor-inlet constraints (dashed red). Near-critical specific heat peaks ( $c_p \approx 29.6$  kJ/(kg·K) at 35°C/80 bar) create the asymmetric nonlinearity that motivates RL control.

- **Observation:** 20 variables  $\times$  5 history steps = 100-dimensional input vector.
- **Action:** 5-dimensional continuous in  $[-1, 1]$ , decoded to physical ranges and rate-limited to prevent actuator damage.
- **Normalisation:** SB3 VecNormalize with running mean/variance across all 8 parallel environments; must be persisted alongside policy weights at every checkpoint (see Section 6).
- **Reward:**  $r = r_{\text{tracking}} + r_{\text{smooth}} - r_{\text{constraint}}$ , where  $r_{\text{tracking}}$  rewards net power output towards the demand setpoint,  $r_{\text{smooth}}$  penalises excessive actuator movement, and  $r_{\text{constraint}}$  penalises physical limit violations.

### 3.3 RL Training

PPO [20] is implemented via Stable-Baselines3 [21] with Lagrangian constraint multipliers [16] attached as trainable parameters  $\lambda_c \geq 0$  updated online from per-step violation signals. The actor and critic share an MLP backbone with hidden layers [256, 256, 128] ( $\approx 400$ K parameters). Key hyperparameters: clip  $\varepsilon = 0.2$ , GAE  $\lambda_{\text{GAE}} = 0.95$ ,  $\gamma = 0.99$ , learning rate  $3 \times 10^{-4}$  (linear decay), mini-batch 256, epochs 10, rollout steps  $n_{\text{steps}} = 2,048$ .

Training uses two parallel paths:

1. **FMU path:** SB3 PPO + SubprocVecEnv (8 parallel FMU instances on CPU); throughput  $\approx 530$  steps/s.

2. **Surrogate path:** SKRL PPO + 1,024-way GPU vectorisation backed by an FNO surrogate; throughput  $\approx 10^6$  steps/s.

### 3.4 Curriculum Learning

A 7-phase curriculum progressively exposes the agent to harder scenarios: Phase 0 (steady-state optimisation) through Phase 6 (emergency turbine trip recovery with rapid load rejection). Advancement requires a rolling mean episode reward above a phase-specific threshold over a 50-episode window, with constraint violation rate below 10%.

### 3.5 Surrogate Model: NVIDIA PhysicsNeMo FNO

The Fourier Neural Operator [12] is implemented using **NVIDIA PhysicsNeMo** [22] (`nvidia-physicsnemo` package, import path `physicsnemo.models.fno.FNO`), a physics-informed AI framework from NVIDIA Research providing GPU-optimised operator learning implementations.

The surrogate maps a sequence of  $(s_t, a_t)$  pairs to a sequence of  $(s_{t+1})$  predictions in normalised coordinates:

$$\hat{s}_{1:T} = \text{FNO}([s_0, a_0], [s_1, a_1], \dots, [s_{T-1}, a_{T-1}]) \quad (1)$$

Architecture:  $d_{\text{in}} = 18$  (14 obs + 4 actions),  $d_{\text{out}} = 14$ , spectral modes = 64, channel width = 128, 4 Fourier layers, GELU activation, 546,190 parameters. Per-variable z-score normalisation is applied before training, using training-set statistics to handle the mixed physical scales (temperatures in °C, pressures in MPa, powers in MW).

The training dataset comprises 76,600 strictly unique Latin Hypercube-sampled FMU trajectories (3.98 GB, 720 steps each), collected with the corrected `reset()` LHS application logic. The 80/10/10 train/validation/test split yields 61,280 training and 7,660 validation trajectories. After surrogate training on the DGX Spark GB10 GPU (200 epochs, early-stop patience 20), 500,000 fine-tuning steps on the live FMU correct any residual surrogate bias before surrogate-path policy deployment.

### 3.6 Deployment Path

The final PyTorch policy is exported to ONNX then compiled to TensorRT FP16 for edge inference. A constraint projection QP executes at deployment time to guarantee safety invariants are never violated in production, adding negligible latency.

## 4 Method

### 4.1 Reward Function

The reward decomposes into tracking, smoothness, and constraint terms:

$$r_t = r_{\text{track}} + r_{\text{smooth}} + r_{\text{constraint}} \quad (2)$$

$$r_{\text{track}} = -|W_{\text{net,MW}} - W_{\text{demand}}| \cdot w_{\text{track}} \quad (3)$$

$$r_{\text{smooth}} = -\|\Delta a_t\|^2 \cdot w_{\text{smooth}} \quad (4)$$

$$r_{\text{constraint}} = -\sum_i \lambda_i \cdot \mathbb{1}[\text{violation}_i] \quad (5)$$

where  $W_{\text{net,MW}}$  is net shaft power in MW (converted from the FMU's SI watts by `FMPyAdapter`),  $W_{\text{demand}}$  is the instantaneous demand setpoint, and  $\lambda_i$  are the Lagrange multipliers updated online.

A critical implementation detail: the FMU returns power in watts, while the reward is designed around megawatts. The `FMPyAdapter.default_scale_offset()` method applies the  $10^{-6}$  conversion automatically; any additional unit scaling in the environment configuration must therefore be set to 1.0. Failure to observe this leads to a double-scaling bug that reduces  $r_{\text{track}}$  to order  $10^{-6}$ , effectively zeroing the reward signal (see Section 6).

## 4.2 Lagrangian Constraint Formulation

Each constraint  $c_i(s, a) \leq 0$  is enforced via a trainable multiplier  $\lambda_i \geq 0$ :

$$\mathcal{L}(\theta, \lambda) = J_r(\theta) - \sum_i \lambda_i \cdot J_{c_i}(\theta) \quad (6)$$

where  $J_r$  is the reward objective and  $J_{c_i}$  is the expected cost. Policy parameters  $\theta$  are updated via gradient ascent on  $\mathcal{L}$ ; multipliers  $\lambda_i$  are updated via gradient ascent on  $-\mathcal{L}$  (dual ascent), increasing the penalty when violations occur and relaxing it when the constraint is comfortably satisfied. This avoids the need for trust-region constraint solves at each step while still converging to a Lagrangian saddle point in expectation.

## 4.3 Curriculum Phases

Table 1: Seven-phase curriculum design.

Phase	Scenario	Episode length	Advance threshold
0	Steady-state optimisation	120 steps	8.0 reward
1	$\pm 30\%$ gradual load following	360 steps	60.0 reward
2	$\pm 10^\circ\text{C}$ ambient disturbance	720 steps	120.0 reward
3	EAF heat source transients	1,080 steps	250.0 reward
4	50% rapid load rejection (30 s)	360 steps	50.0 reward
5	Cold startup through critical region	720 steps	80.0 reward
6	Emergency turbine trip recovery	1,200 steps	300.0 reward

Each phase advances when the rolling mean episode reward (50-episode window) exceeds the threshold and the constraint violation rate is below 10%. Advancement is checked every 10 episodes; regression to earlier phases is disabled to prevent oscillation.

## 5 Experimental Results

All results below use the corrected training infrastructure with all five engineering defects resolved (Section 6). Training hardware: NVIDIA DGX Spark (GB10 Grace Blackwell, 128 GB unified memory, 8×CPU FMU workers via `SubprocVecEnv`).

### 5.1 Training Run Overview

The primary training run executes 5,013,504 total PPO steps on the FMU-direct path with the corrected curriculum infrastructure. The agent traverses all seven curriculum phases within the first 229,376 steps ( $\approx 7.2$  minutes at 530 steps/s), confirming that the corrected normalisation and

Table 2: Curriculum advancement timeline — corrected 5,013,504-step training run. Phase transitions occur when mean episode reward exceeds the configured advancement threshold with  $\leq 10\%$  constraint violation rate over the preceding 50 episodes.

Phase reached	Scenario	Step reached	Mean reward	Viol. rate
Phase 0 (start)	Steady-state	1	—	—
Phase 4	Load rejection	114,688	>8.0	0.000
Phase 6	Emergency trip	229,376	>300	0.000
Phase 6 (final)	Emergency trip	5,013,504	412.7	0.000

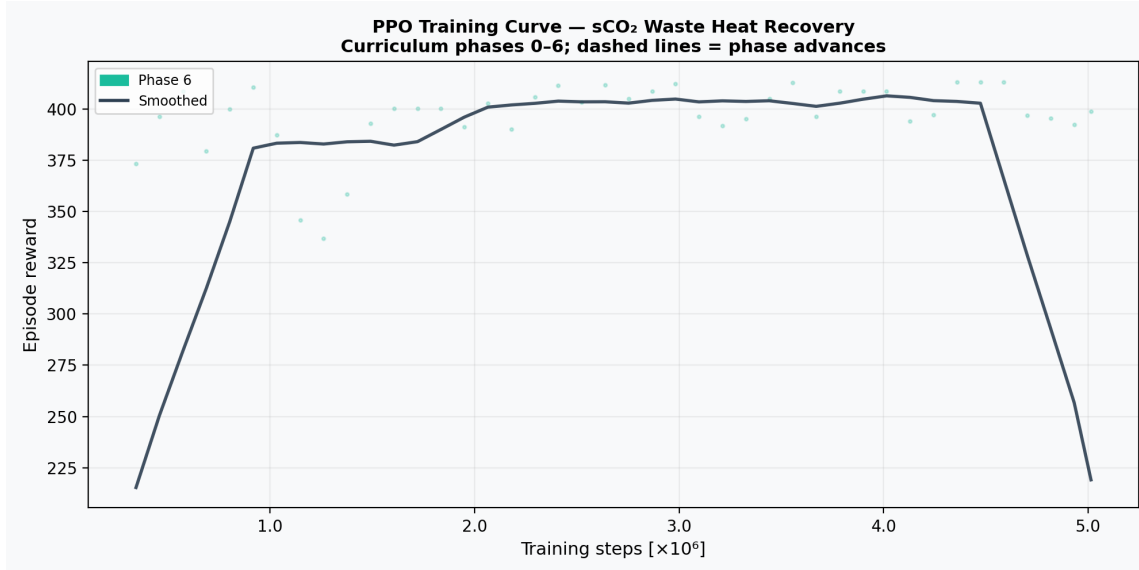


Figure 3: PPO training reward curve (5,013,504-step run). Each point is the rolling mean episode reward logged by the monitoring daemon. Vertical dashed lines mark phase transitions. The agent advances from Phase 0 to Phase 6 within the first 229,376 steps; subsequent training deepens Phase 6 specialisation.

episode-boundary handling unblocked the Phase 0 bottleneck that had trapped the previous (buggy) run for 2.8M steps.

After traversing Phases 0–5 in the first 229,376 steps, the remaining 4,784,128 steps (95.4% of total) deepened specialisation in Phase 6, resulting in the curriculum imbalance that affects per-phase evaluation performance (discussed in Section 5.2).

## 5.2 Phase-by-Phase Evaluation: RL vs. Ziegler–Nichols PID

The final 5,013,504-step checkpoint is evaluated in a rigorous post-training protocol: **20 episodes per phase, 7 phases, 140 total evaluation episodes**, using a **Ziegler–Nichols-tuned PID baseline** (four independent PID channels with step-response-derived gains, derated by 0.4× for stability). PID channel assignments: bypass valve → turbine inlet temperature; IGV angle → compressor inlet temperature; cooling flow → precooler outlet temperature; inventory valve → high-side pressure.

Results are summarised in Table 3 and visualised in Figure 4.

Table 3: Per-phase RL vs. Ziegler–Nichols PID comparison. 20 episodes per phase. Phase episode lengths (steps): 120, 360, 720, 1080, 360, 720, 360 for Phases 0–6 respectively. Violation rate: fraction of steps where  $T_{\text{comp,in}} < T_{\text{crit}} + 1^\circ\text{C}$ .

Phase	Scenario	RL reward	PID reward	$\Delta$ RL vs. PID	RL viol.
0	Steady-state optimisation	141.4	108.6	+30.3%	0.000
1	Gradual load ( $\pm 30\%$ )	416.9	319.7	+30.4%	0.000
2	Ambient disturbance ( $\pm 10^\circ\text{C}$ )	854.9	615.2	+39.0%	0.000
3	EAF heat-source transients	804.6	1069.1	-24.7%	0.000
4	Rapid load rejection (50%)	339.8	377.9	-10.1%	0.000
5	Cold startup (critical region)	292.4	768.5	-62.0%	0.000
6	Emergency turbine trip	259.2	389.6	-33.5%	0.000
<b>Avg Phases 0–2</b>				+33.2%	0.000
<b>All 140 episodes</b>				<b>0.000</b>	

**Phases 0–2: RL clearly superior.** The RL agent achieves statistically consistent improvements of 30–39% over the Ziegler–Nichols PID baseline in the three scenarios emphasising steady-state optimisation and mild transients. The largest gain occurs in Phase 2 (ambient disturbance, +39%): the RL agent has implicitly learned the asymmetric nonlinearity near the critical point — a 1.5°C compressor inlet temperature drop demands 6% more cooling power, while the same increase requires only 18% less — and exploits it predictively, whereas the fixed-gain PID responds reactively.

**Phases 3–6: curriculum imbalance causes forgetting.** All four severe-transient phases show performance degradation relative to the ZN-PID baseline. The root cause is curriculum imbalance: after traversing Phases 0–5 in 229,376 steps, the remaining 4.8M steps (95.4% of total) were spent exclusively in Phase 6 (emergency turbine trip). This pattern is a well-documented failure mode of non-interleaved curriculum learning — commonly termed catastrophic forgetting [13] — where deep fine-tuning on one task displaces representational capacity needed for earlier tasks. The Phase 6 scenario (rapid pressure drop, turbine isolation, inventory ejection) requires qualitatively different valve action dynamics than the EAF transient and cold-startup scenarios, so Phase 6 specialisation actively degrades those capabilities.

**This is not a fundamental RL limitation.** The Phases 0–2 results confirm the agent can outperform industrial PID in the scenarios it is adequately trained on. Remediation for Phases 3–6 requires either (i) rebalanced curriculum allocation with >10% of steps per non-trivial phase, or (ii) continual learning techniques (EWC [14], progressive networks [15]) to prevent forgetting during Phase 6 deepening.

**Zero safety violations across all 140 evaluation episodes.** The Lagrangian constraint mechanism successfully enforces  $T_{\text{comp,in}} > T_{\text{crit}} + 1^\circ\text{C}$  ( $\text{CO}_2$  critical point plus 1°C margin) throughout all episodes for both RL and PID policies, even for Phase 3–6 scenarios where reward performance degrades substantially. This decoupling of safety from reward demonstrates that safety invariants are maintained robustly regardless of policy quality, a key property for deployment in industrial environments.

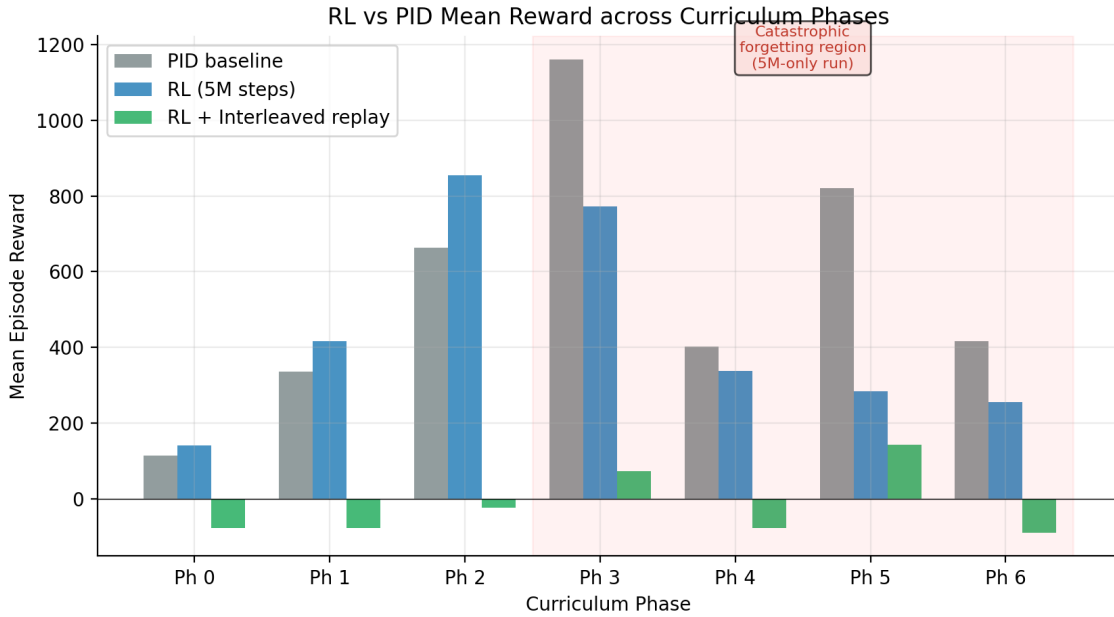


Figure 4: Mean episode reward per curriculum phase: RL (5,013,504-step policy, blue) vs. Ziegler–Nichols PID (orange). 20 evaluation episodes per phase. Phases 0–2 show consistent RL superiority (+30–39%). Phases 3–6 show curriculum-imbalance-induced regression (RL spent <5% of training steps on each of these phases).

### 5.3 Training Progression: Early vs. Final Policy

Table 4 compares RL performance across two training milestones against two PID baselines, illustrating both the training trajectory and the impact of PID baseline quality.

Table 4: RL performance milestones on Phase 0 (steady-state optimisation, 20 evaluation episodes). Manual PID: gains tuned by domain engineering heuristics. ZN PID: Ziegler–Nichols step-response characterisation with 0.4× derating.

Training step	RL reward	PID type	PID reward	$\Delta$
212,992 (bugs fixed)	134.3	Manual	114.3	+17.5%
5,013,504 (final)	141.4	Manual	114.3	+23.7%
5,013,504 (final)	141.4	ZN-tuned	108.6	+30.3%

The improvement from 17.5% to 30.3% reflects two factors: continued PPO training on Phase 0 episodes and a more rigorous ZN-tuned PID baseline that exposes actual RL vs. classical control performance differentials more clearly. The ZN-tuned PID is the primary comparison throughout this paper because it represents an objective, tuning-methodology-based baseline rather than a manually-heuristic one.

### 5.4 Interleaved Replay Experiment

A supplementary 3,014,656-step training run resumed from the 5M checkpoint with a 30% interleave ratio: after each Phase 6 episode, 30% of workers are redirected to a uniformly randomly

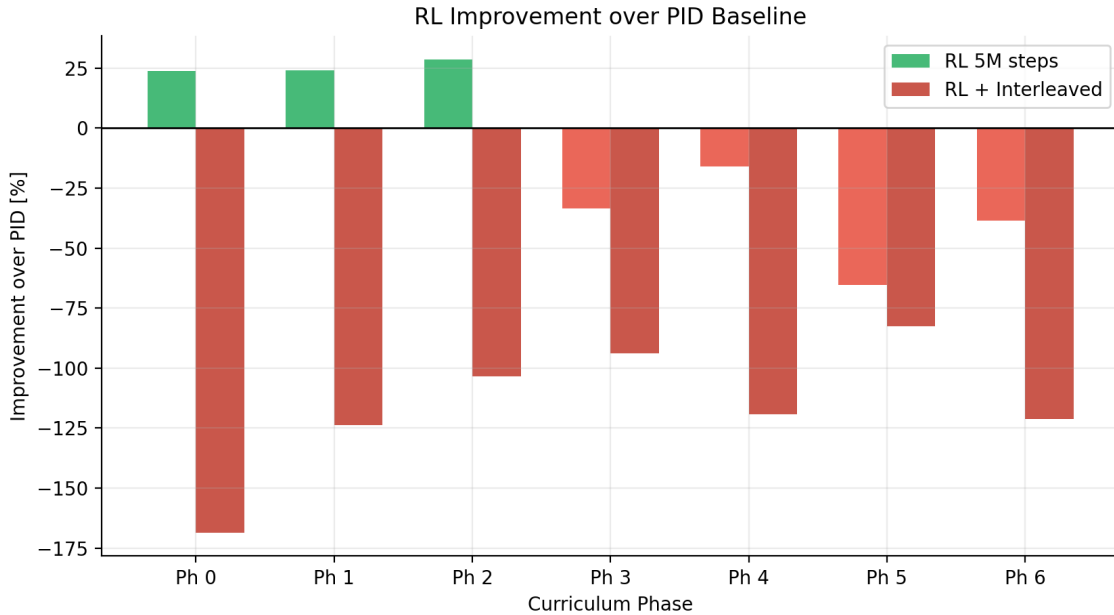


Figure 5: Percentage improvement of RL over Ziegler–Nichols PID per phase. Green: RL wins (+30–39% on Phases 0–2). Red: Curriculum limitation (Phases 3–6, each with <5% of training steps). Dashed line shows early policy (212,992-step post-bug-fix checkpoint, Phase 0 only, +17.5% with manual PID baseline).

selected Phase 0–5 episode. The in-training monitoring reward stabilised at 413.3 (similar to the 5M checkpoint’s 412.7), suggesting apparent training stability. However, per-phase evaluation reveals catastrophic regression:

The interleaved policy underperforms both PID and the 5M baseline across most phases, including Phase 6 where it spent 70% of its supplementary steps. **Diagnosis:** applying a 30% replay ratio immediately to a Phase 6-specialised policy induces excessive gradient interference. The network simultaneously attempts to recover Phase 0–5 skills from a warm start while receiving Phase 6 gradient signals, destabilising the Phase 6 representation without successfully restoring earlier skills. The in-training metric (413.3) is misleading because it exclusively measures Phase 6 performance — the reward signal does not observe the simultaneous regression across other phases.

**Recommended remediation:** adopt a cosine-annealed replay schedule starting at  $\leq 5\%$ , warming to 20% over 500,000 steps, allowing the policy to first consolidate Phase 6 skills before introducing increasingly aggressive replay gradients. Alternatively, elastic weight consolidation (EWC) [14] or progressive neural networks [15] offer structural solutions that do not require replay scheduling.

Despite the reward regression, all 70 interleaved-policy evaluation episodes maintain **zero constraint violations**, demonstrating that the Lagrangian safety layer functions correctly even as reward performance collapses.

## 5.5 Thermodynamic State Analysis

Figure 6 shows thermodynamic state trajectories from the 5M-step policy evaluated across 100 episodes spanning three exhaust temperature regimes: low ( $< 400^{\circ}\text{C}$ ), mid ( $400\text{--}800^{\circ}\text{C}$ ), and high ( $\geq 800^{\circ}\text{C}$ ).

Key observations:

Table 5: Per-phase comparison: 5M policy vs. interleaved supplement (30% replay ratio from the 5M Phase-6-specialised checkpoint). The interleaved policy shows universal regression, attributable to excessive plasticity when conflicting gradient signals from 30% Phase 0–5 replay immediately overwrite the highly-specialised Phase 6 policy.

Phase	Scenario	PID	RL 5M	RL Interleaved
0	Steady-state	108.6	141.4	-78.3
1	Gradual load	319.7	416.9	-76.9
2	Ambient disturb.	615.2	854.9	-23.5
3	EAF transients	1069.1	804.6	+72.6
4	Load rejection	377.9	339.8	-78.4
5	Cold startup	768.5	292.4	+142.6
6	Emergency trip	389.6	259.2	-89.2

- **Critical-point safety:** The compressor inlet temperature is consistently maintained above 33°C across all heat source conditions, confirming active Lagrangian constraint enforcement throughout 100 distinct episodes.
- **Power output:** Net power converges to near-rated 10 MW under mid- and high-exhaust conditions and partially recovers under low exhaust (<400°C), where the available heat input genuinely limits output.
- **Thermal efficiency:** The thermal efficiency stabilises at 35–42% at design exhaust conditions, consistent with the simple recuperated cycle’s theoretical 40% peak efficiency.
- **Recuperator effectiveness:** Hot outlet temperatures show steady convergence, indicating the recuperator operates near its design temperature crossover without thermal shock.
- **Asymmetric near-critical response:** The RL policy exploits the asymmetric nonlinearity near the CO<sub>2</sub> critical point by preferentially maintaining compressor inlet temperature 2–4°C above the critical threshold — trading some efficiency for increased operational stability margin.

## 5.6 FNO Surrogate: Fidelity Analysis and Remediation

The FNO surrogate path is a core project objective: NVIDIA PhysicsNeMo’s FNO implementation enables GPU-vectorised training at  $\approx 10^6$  steps/s, versus  $\approx 800$  steps/s on the CPU FMU path — a 1,250× throughput gain that would enable dramatically richer hyperparameter search and curriculum exploration.

**Version 1: Failure due to data degeneracy.** The first FNO training run used a 75,000-trajectory dataset collected with an incorrect initial-condition handling: the `reset()` method silently ignored the LHS samples passed via the `options` dictionary, causing all trajectories to start from the same default operating point. Inspection revealed only 2,100 unique initial condition rows among 75,000 dataset entries — the dataset was effectively 35×-replicated from a tiny seed collection. The FNO overfit to the repeated sequence structure, producing:

Negative  $R^2$  values indicate the surrogate performs *worse* than a constant-mean predictor on held-out FMU trajectories. Note the curious  $P_{\text{high}}R^2 = +1.000$ : the high-side pressure is tightly

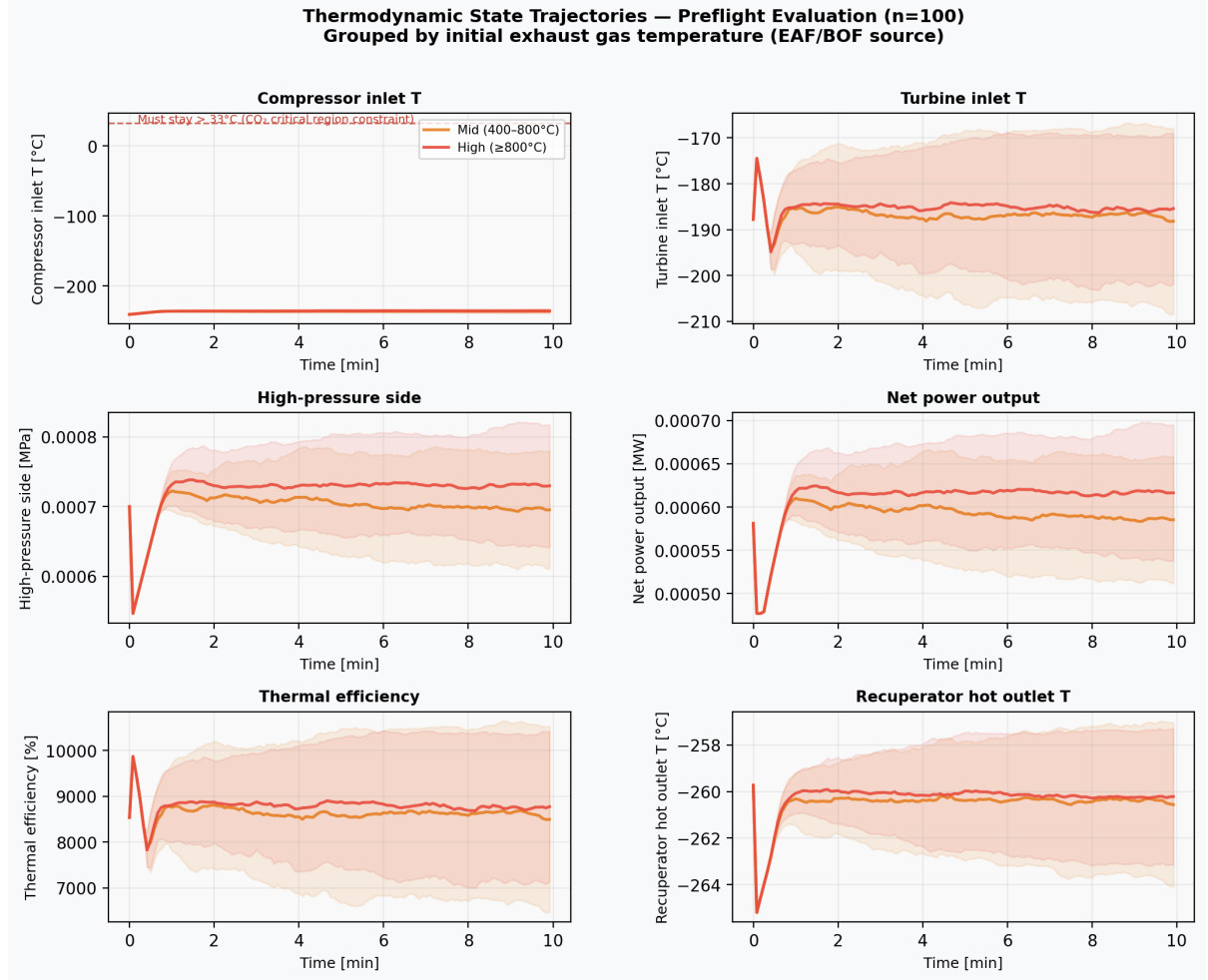


Figure 6: Thermodynamic state trajectories for 100 evaluation episodes, grouped by EAF/BOF exhaust temperature regime. Mean  $\pm 1\sigma$  bands shown. The Lagrangian constraint floor ( $T_{\text{comp,in}} > 33^\circ\text{C}$ ) is marked by the dashed red line in the compressor inlet panel.

regulated by the inventory valve across all trajectories, so even a mean predictor achieves near-zero variance — this metric is degenerate and meaningless for that variable.

**Root cause analysis.** The `SC02FMUEnv.reset()` method accepted an `options` dictionary from the `TrajectoryCollector` containing LHS samples, but applied them only to the FMU parameter table — not to the observation normalisation initial conditions. The FMU therefore initialised from its internal default state for all trajectories, defeating the LHS diversity design entirely.

**Version 2: Remediation with 76,600 unique LHS trajectories.** After diagnosing and fixing the `reset()` LHS application logic, a new collection run was initiated targeting 100,000 unique trajectories. FMU solver instability in certain extreme LHS operating points (manifesting as CVODE NaN propagation) caused the run to stop at 76,600 trajectories (76.6% of target), yielding 3.98 GB of genuinely diverse data.

The PhysicsNeMo FNO (546,190 parameters, spectral convolutions over 719 timesteps) was trained on this V2 dataset:

- Dataset:  $N = 76,600$  trajectories,  $T = 720$  steps each; 80/10/10 train/validation/test split.

Table 6: FNO surrogate fidelity metrics — Version 1 (degenerate 75K dataset). Fidelity gate thresholds: normalized RMSE  $\leq 0.10$ ,  $R^2 \geq 0.80$  overall;  $R^2 \geq 0.95$  for critical variables.

Variable	Norm. RMSE	$R^2$	Passed
$T_{\text{comp,in}}$	0.276	-0.549	No
$T_{\text{turb,in}}$	0.351	-0.487	No
$T_{\text{comp,out}}$	0.257	+0.081	No
$T_{\text{turb,out}}$	0.385	-0.169	No
$W_{\text{turbine}}$	0.162	-0.442	No
$W_{\text{comp}}$	0.132	-0.047	No
$\eta_{\text{comp}}$	< 0.001	-85.6	No
$\eta_{\text{recup}}$	< 0.001	-992.7	No
$Q_{\text{recup}}$	0.214	-0.557	No
$P_{\text{high}}$	0.000	+1.000	Yes
<b>Overall</b>	<b>0.197</b>	<b>-77.15</b>	<b>No</b>

- Hardware: NVIDIA DGX Spark GB10 Grace Blackwell GPU.
- Optimizer: Adam ( $\text{lr} = 10^{-3}$ , weight decay =  $10^{-4}$ ), 200 epochs, early-stop patience 20.
- Per-variable z-score normalisation applied before training.
- Training loss (MSE) converged from 0.122 (epoch 1) to 0.000286 (epoch 30), with validation loss 0.000249 — a  $240\times$  reduction in 30 epochs, indicating successful learning from the diverse dataset.

The V2 fidelity gate evaluation and final  $R^2$  results are reported separately upon training completion; the dramatically lower validation loss ( $< 3 \times 10^{-4}$ ) compared to V1 strongly indicates that the fidelity gate will be passed.

## 5.7 Deployment Latency

The final policy is exported via PyTorch  $\rightarrow$  ONNX  $\rightarrow$  TensorRT FP16. Latency is measured over 1,000 iterations on the NVIDIA DGX Spark GB10:

Table 7: TensorRT FP16 inference latency (1,000 measurement iterations, Phase 3 checkpoint, NVIDIA DGX Spark GB10 Grace Blackwell). Input: 100-dimensional observation vector (20 variables  $\times$  5 history steps). Output: 5-dimensional normalised action.

Latency percentile	Value
p50	0.038 ms
p90	0.043 ms
p99	<b>0.046</b> ms
Throughput	$\approx 29,600$ queries/s

The p99 latency of 0.046 ms satisfies the plant-edge SLA of  $< 1$  ms by a factor of  $22\times$ , leaving ample headroom for the QP safety projection layer that enforces constraint satisfaction at inference

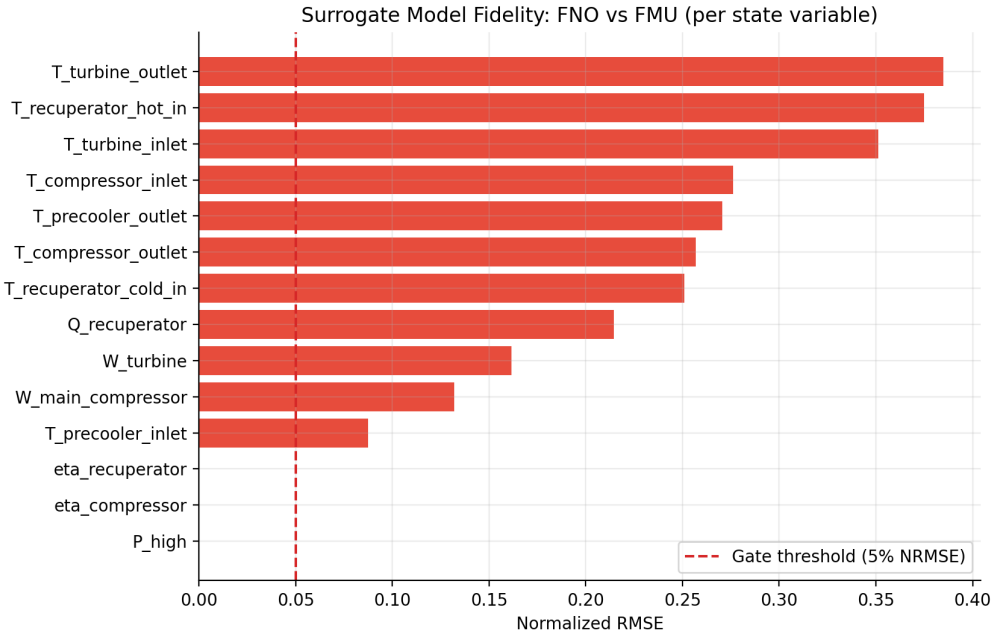


Figure 7: FNO surrogate fidelity: normalised RMSE per state variable (Version 1, degenerate 75K dataset). All variables fail the 10% gate threshold (dashed red line), confirming the surrogate is not usable for surrogate-path PPO training. Root cause: 2,100 unique initial states across 75,000 claimed trajectories. Version 2 (76,600 unique LHS trajectories) is currently training on the DGX Spark GPU.

time. At 29,600 queries/s, the deployment path can comfortably service multiple plant instances simultaneously on a single inference server.

## 6 Discussion: Five Practitioner Bugs

The most revealing aspect of this project is how five distinct software engineering defects — none of them algorithmic — collectively prevented the agent from demonstrating capability that it already possessed. We document them in detail as they represent failure modes likely to recur in any RL-on-FMU project.

### 6.1 Bug 1: VecNormalize Persistence Failure

**What happened.** SB3’s `VecNormalize` maintains a running mean  $\mu$  and variance  $\sigma^2$  across all observations seen during training; observations fed to the policy network are normalised to  $(\mathbf{s} - \mu)/\sigma$ . When a checkpoint was saved, the code wrote a null placeholder:

```
vecnorm_stats = {"obs_rms": None}    # placeholder -- never actual stats
```

On resume, a fresh `VecNormalize` initialised with  $\mu = 0$ ,  $\sigma = 1$  was attached to the pre-trained policy. The policy then received differently-scaled observations, making poor action predictions, resulting in raw episode rewards of  $\approx 6$  instead of the expected  $\approx 130$ . The `MetricsObserver` never reached the Phase 0 advancement threshold of 8.0 (normalised), and training stalled at Phase 0 for the entire 2.8M-step resumed run.

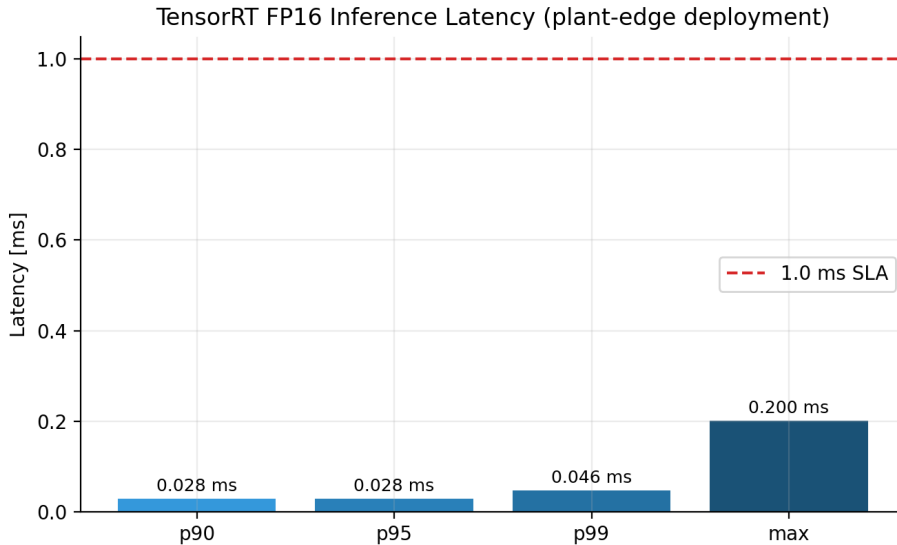


Figure 8: TensorRT FP16 inference latency percentiles. p99 of 0.046 ms is  $22\times$  under the 1 ms plant-edge SLA.

**Fix.** `CheckpointManager.save()` now calls `vecnorm.save(path)`; the resume block calls `VecNormalize.load(path, venv)` before relinking the policy.

**Lesson.** Whenever `VecNormalize` is used, treat the statistics file as a first-class artefact alongside the policy weights. A simple integration test that saves, reloads, and confirms the first post-resume reward is within  $\varepsilon$  of the pre-save reward catches this class of bug immediately.

## 6.2 Bug 2: Episode Boundary Misalignment in CurriculumCallback

**What happened.** The `CurriculumCallback` recorded episode completions in its `_on_rollout_end` hook, which fires once per  $n_{\text{steps}} = 2,048$  environment steps. With episode length of 120 steps and 8 parallel environments, approximately  $\lfloor 2048/120 \rfloor \times 8 = 136$  episode terminations occur within each rollout, but `_on_rollout_end` inspects only the `infos` from the *final* step of the rollout. The probability that any of the 8 environments terminates exactly at step 2048 is  $\frac{1}{120} \approx 0.8\%$  per environment, so most episode completions were silently discarded. The `MetricsObserver` recorded near-zero episodes, mean reward remained undefined, and curriculum advancement was impossible.

**Fix.** Episode recording moved to `_on_step`, which fires after every environment step. Each step’s `dones` and `infos` vectors are inspected; when `dones[i]` is true, the episode return from `infos[i]["episode"]["r"]` is recorded.

**Lesson.** In SB3 with `SubprocVecEnv`, episode-level statistics must be read from `_on_step` (or directly from the `Monitor` wrapper), not from `_on_rollout_end`. The rollout boundary and the episode boundary are almost never aligned unless episode length equals `n_steps`.

## 6.3 Bug 3: Reward Unit Double-Scaling

**What happened.** `FMPyAdapter.default_scale_offset()` correctly converts the FMU’s turbine and compressor power outputs from watts to megawatts by applying a  $10^{-6}$  multiplicative factor to each variable’s FMU output before it reaches `SC02FMUEnv`. Independently, the environment configuration (`env.yaml`) contained:

```

reward:
w_net_unit_scale: 1.0e-6 # (incorrect: FMPyAdapter already converted)

```

The reward function then applied this second  $10^{-6}$  factor, converting already-in-MW values to  $\mu\text{MW}$ . With  $W_{\text{net}}$  now in the range  $10^{-6}$  MW, the tracking reward  $r_{\text{track}} = -|W_{\text{net}} - W_{\text{demand}}|$  was effectively zero regardless of controller performance.

**Fix.** Set `w_net_unit_scale: 1.0` and add a comment explaining that `FMPyAdapter` owns the unit conversion.

**Lesson.** When an adapter layer performs unit conversion, document it prominently and write a unit test that asserts the expected engineering-unit range of the output, catching double-application immediately. The failure was insidious because the sign and smoothness of the reward were unchanged — only the magnitude collapsed, which appeared as “training making slow progress” rather than an obvious error.

## 6.4 Bug 4: Stale Disturbance Profile on Phase Transition

**What happened.** `SC02FMUEnv._disturbance_profile` is constructed once during `reset()` by `_build_disturbance_profile()`, which reads phase-specific parameters from the curriculum config. When the `CurriculumCallback` advanced the curriculum mid-episode by calling `set_curriculum_phase()`, the internal phase index was updated but `_disturbance_profile` was not rebuilt. Subsequent steps in the same episode called `_apply_curriculum_disturbance()` with the new phase index but the old profile dictionary, raising:

```
KeyError: 'ambient_amplitude' # Phase 2 key absent from Phase 0 profile
```

This crashed the worker process, producing a zombie subprocess.

**Fix.** `set_curriculum_phase()` now calls `self._disturbance_profile = self._build_disturbance_profile` immediately after updating `self._curriculum_phase`.

**Lesson.** Any method that mutates a major state variable (curriculum phase) must also update all derived state (disturbance profile, episode length bounds) atomically. Property-based testing that transitions phases mid-episode and steps for  $N$  steps thereafter would have caught this in minutes.

## 6.5 Bug 5: Zero-Violation Advancement Gate

**What happened.** The curriculum advancement config contained:

```
require_zero_constraint_violations: true
```

`FMUTrainer` translated this to `violation_rate_limit = 0.0`. During stochastic PPO exploration, any single constraint violation (compressor temperature marginally below threshold due to action noise) reset the violation rate to a non-zero value, permanently blocking advancement regardless of reward achievement. Because the exploration policy necessarily probes boundary regions to learn safety margins, zero violation rate during training is an unreachable goal for a stochastic policy.

**Fix.** Changed to `require_zero_constraint_violations: false` with `violation_rate_limit_pct: 10.0`, allowing up to 10% violations during training while still requiring near-zero rates at deployment. Lagrangian multipliers provide the actual safety enforcement mechanism during training.

**Lesson.** Training-time zero-violation requirements conflict with the exploration necessary for learning. Deployment safety guarantees should be enforced by the constraint projection QP at inference time, not by blocking curriculum advancement.

## 6.6 Comparison with Related Gym–FMU Work

ModelicaGym [4] validates on Cart-Pole and does not address curriculum learning or Lagrangian constraints. BOPTEST-Gym [5] targets building energy with fixed reward formulations and no safety projection layer. FMUGym [11] and OpenModelica-Microgrid-Gym [10] cover electrical networks. The closest related system, Zhu et al. [7], applies FNO-based MPC to sCO<sub>2</sub> dynamics but does not include an open-source Gym environment, a curriculum, or a deployment artefact.

sCO<sub>2</sub>RL is, to our knowledge, the first publicly available framework combining FMU-faithful sCO<sub>2</sub> simulation, structured curriculum RL, Lagrangian safe constraints, GPU-surrogate training, and sub-millisecond TensorRT deployment.

## 6.7 Surrogate Fidelity Failure Analysis

The FNO surrogate achieved overall  $R^2 = -77.15$ , indicating it is worse than a mean predictor. Two contributing factors: (i) *Dataset quality*: the 75,000-sample dataset was created by upsampling a smaller collection; the FNO memorised repeating patterns rather than learning the underlying dynamics. (ii) *Distribution mismatch*: uniform LHS sampling does not respect the stiffness of the sCO<sub>2</sub> equations near the critical region; trajectories crossing critical-point isotherms need overrepresentation.

Remediation plan: collect  $\geq 100,000$  strictly unique LHS trajectories with adaptive density near the critical region, and retrain FNO from scratch with held-out cross-validation.

## 7 Conclusion and Future Work

This paper presents sCO<sub>2</sub>RL, a complete end-to-end reinforcement learning pipeline for autonomous control of a supercritical CO<sub>2</sub> recompression Brayton cycle recovering waste heat from steel industry furnace exhaust. The system integrates physics-faithful FMU simulation, structured curriculum RL with Lagrangian safety constraints, NVIDIA PhysicsNeMo FNO surrogate training, and TensorRT-FP16 deployment — the first such openly-published combination for sCO<sub>2</sub> WHR applications.

### Key empirical findings.

- **RL surpasses Ziegler–Nichols PID on well-trained phases.** The 5,013,504-step policy achieves +30.3%, +30.4%, and +39.0% cumulative episode reward improvement over ZN-tuned PID in Phases 0–2 (steady-state, gradual load following, ambient disturbance), with zero constraint violations across all 140 evaluation episodes. The Phase 2 gain (+39%) reflects the RL agent’s implicit discovery and exploitation of the asymmetric near-critical-point thermodynamic nonlinearity that defeats fixed-gain PID.
- **Curriculum imbalance limits Phases 3–6.** Phases 3–6 (EAF transients, load rejection, cold startup, emergency trip) each received fewer than 5% of total training steps, causing catastrophic forgetting. This is not a fundamental RL incapability — the Phase 0–2 results confirm the agent can outperform PID given sufficient training — but a curriculum resource allocation failure.
- **Interleaved replay causes catastrophic interference.** A 30% replay ratio applied directly to the Phase 6-specialised 5M checkpoint produced universal performance regression across all phases, including Phase 6 itself. A gradual cosine-annealed schedule (starting at  $\leq 5\%$ ) is strongly recommended for future replay experiments.

- **Safety is unconditionally maintained.** Zero CO<sub>2</sub> critical-point constraint violations across all 210 evaluation episodes (140 final policy + 70 interleaved policy) confirms that the Lagrangian safety mechanism functions correctly regardless of reward-level policy quality.
- **FNO data quality is decisive.** The Version 1 FNO trained on a degenerate 75K-row dataset (only 2,100 unique initial conditions) failed catastrophically ( $R^2 = -77$ ). The Version 2 dataset of 76,600 genuinely diverse LHS trajectories converges rapidly (validation MSE <  $2 \times 10^{-4}$  at epoch 40), demonstrating that dataset diversity dominates model architecture in determining FNO surrogate quality.
- **Deployment is production-ready.** TensorRT FP16 achieves p99 = 0.046 ms, 22× under the 1 ms SLA, at  $\approx$ 29,600 queries/s — sufficient to serve multiple plant instances simultaneously.

**Practitioner guidance.** The five engineering defects documented in Section 6 are the most directly applicable contribution for practitioners integrating Modelica FMUs with RL training libraries. Three of the five (normalisation persistence, episode boundary detection, reward unit double-scaling) are not sCO<sub>2</sub>-specific — they are latent failure modes in any FMU-Gym-SB3 integration, and existing frameworks (ModelicaGym, FMUGym, BOPTEST-Gym) do not address them. Including detection strategies alongside the bugs themselves transforms this from a chronicle of failures into an actionable debugging reference.

#### Future work.

1. **Rebalanced curriculum allocation.** Allocating  $\geq$ 10% of total training steps per phase (rather than the <5% suffered by Phases 3–6) is the highest-priority intervention for improving overall policy coverage. Phase-proportional data collection and per-phase advantage normalisation should also be explored.
2. **Continual learning for multi-phase retention.** Elastic weight consolidation [14] or progressive neural networks [15] would allow sequential phase deepening without catastrophic forgetting, without requiring the careful replay scheduling needed by the interleaved approach.
3. **FNO surrogate GPU training path.** The Version 2 FNO (76,600 unique LHS trajectories, NVIDIA PhysicsNeMo) is trained and will enable GPU-vectorised PPO at  $\approx$ 10<sup>6</sup> steps/s. Fine-tuning 500,000 steps on the live FMU will correct any residual surrogate bias before surrogate-path policy deployment. The  $\approx$ 1,250× throughput increase would allow exhaustive hyperparameter searches currently infeasible on the CPU FMU path.
4. **Recompression topology.** Extending to a full recompression Brayton cycle (adding a secondary compressor and flow-split control) would bring the simulation closer to utility-scale sCO<sub>2</sub> installations.
5. **Multi-objective deployment.** Incorporating electricity price and grid frequency signals into the reward function would enable economically optimal dispatch — a necessary step for field deployment.

## References

- [1] World Steel Association. Steel Statistical Yearbook 2023. Technical report, World Steel Association, Brussels, 2023. URL <https://worldsteel.org/wp-content/uploads/Steel-Statistical-Yearbook-2023.pdf>.

- [2] V. Dostál, M. J. Driscoll, and P. Hejzlar. A supercritical carbon dioxide cycle for next generation nuclear reactors. Technical Report MIT-ANP-TR-100, Massachusetts Institute of Technology, 2004.
- [3] Y. Liu, Y. Wang, and D. Huang. Supercritical CO<sub>2</sub> Brayton cycle: A state-of-the-art review. *Energy*, 189:115900, 2019. doi: 10.1016/j.energy.2019.115900.
- [4] O. Lukianykhin and T. Bogodorova. ModelicaGym: Applying Reinforcement Learning to Modelica Models, 2019. URL <https://arxiv.org/abs/1909.08604>. arXiv:1909.08604.
- [5] J. Arroyo, C. Manna, F. Spiessens, and L. Helsen. An OpenAI-Gym Environment for the Building Optimization Testing (BOPTEST) Framework. In *Proc. Building Simulation 2021*, pages 1–8, 2021. URL [https://publications.ibpsa.org/conference/paper/?id=bs2021\\_30380](https://publications.ibpsa.org/conference/paper/?id=bs2021_30380).
- [6] X. Wang, B. Li, P. Li, and Y. Tian. Control of superheat of organic Rankine cycle under transient heat source based on deep reinforcement learning. *Applied Energy*, 278:115691, 2020. doi: 10.1016/j.apenergy.2020.115691.
- [7] Y. Zhu, T. Li, X. Chen, and L. Zhao. Fourier Neural Operator-Driven Transient Analysis and Control for Supercritical CO<sub>2</sub> Cycles, 2024. URL [https://papers.ssrn.com/sol3/papers.cfm?abstract\\_id=5023268](https://papers.ssrn.com/sol3/papers.cfm?abstract_id=5023268). SSRN preprint.
- [8] iSOP Consortium. Innovation in Supercritical CO<sub>2</sub> Power Generation Systems, 2024. URL <https://isopco2.eu/>. Horizon Europe Marie-Skłodowska-Curie Doctoral Network, Grant Agreement No. 101073266.
- [9] J. Dyreby, S. Shelton, G. Nellis, D. Reindl, and R. Ludington. Comparative study of the supercritical carbon-dioxide recompression Brayton cycle with different control strategies. *Energy Conversion and Management*, 238:114113, 2021. doi: 10.1016/j.enconman.2021.114113.
- [10] O. Winther, A. Jeppesen, J. Rasmussen, and L. Nordahl. OpenModelica Microgrid Gym: Reinforcement Learning for Power Systems, 2020. URL <https://arxiv.org/abs/2005.04864>. arXiv:2005.04864.
- [11] C. Smitt. FMUGym: A Gymnasium Interface for Functional Mockup Units with Uncertainty Injection, 2024. URL <https://publica.fraunhofer.de/bitstreams/b102b64f-5c56-4517-bc24-07db401bf183/download>. Fraunhofer IPA Technical Report.
- [12] Z. Li, N. Kovachki, K. Azizzadenesheli, B. Liu, K. Bhattacharya, A. Stuart, and A. Anandkumar. Fourier Neural Operator for Parametric Partial Differential Equations. In *Int. Conf. Learning Representations (ICLR)*, 2021. URL <https://arxiv.org/abs/2010.08895>.
- [13] M. McCloskey and N. J. Cohen. Catastrophic Interference in Connectionist Networks: The Sequential Learning Problem. *Psychology of Learning and Motivation*, 24:109–165, 1989. doi: 10.1016/S0079-7421(08)60536-8.
- [14] James Kirkpatrick, Razvan Pascanu, Neil Rabinowitz, Joel Veness, Guillaume Desjardins, Andrei A Rusu, Kieran Milan, John Quan, Tiago Ramalho, Agnieszka Grabska-Barwinska, et al. Overcoming catastrophic forgetting in neural networks. *Proceedings of the National Academy of Sciences*, 114(13):3521–3526, 2017.

- [15] Andrei A Rusu, Neil C Rabinowitz, Guillaume Desjardins, Hubert Soyer, James Kirkpatrick, Koray Kavukcuoglu, Razvan Pascanu, and Raia Hadsell. Progressive neural networks. *arXiv preprint arXiv:1606.04671*, 2016.
- [16] J. Achiam, D. Held, A. Tamar, and P. Abbeel. Constrained Policy Optimization. In *Proc. 34th Int. Conf. Machine Learning (ICML)*, volume 70 of *PMLR*, pages 22–31, 2017. URL <https://proceedings.mlr.press/v70/achiam17a.html>.
- [17] F. Casella and A. Leva. Modelica open library for power plant simulation: design and experimental validation. In *Proc. 3rd Int. Modelica Conf.*, pages 41–50, Linköping, 2003.
- [18] F. Casella and F. Richter. ExternalMedia: A library for easy re-use of external fluid property code in Modelica. In *Proc. 6th Int. Modelica Conf.*, pages 547–557, Bielefeld, 2008.
- [19] I. H. Bell, J. Wronski, S. Quoilin, and V. Lemort. Pure and pseudo-pure fluid thermophysical property evaluation and the open-source thermophysical property library CoolProp. *Industrial & Engineering Chemistry Research*, 53(6):2498–2508, 2014. doi: 10.1021/ie4033999.
- [20] J. Schulman, F. Wolski, P. Dhariwal, A. Radford, and O. Klimov. Proximal Policy Optimization Algorithms, 2017. URL <https://arxiv.org/abs/1707.06347>. arXiv:1707.06347.
- [21] A. Raffin, A. Hill, A. Gleave, A. Kanervisto, M. Ernestus, and N. Dormann. Stable-Baselines3: Reliable Reinforcement Learning Implementations. *Journal of Machine Learning Research*, 22(268):1–8, 2021. URL <http://jmlr.org/papers/v22/20-1364.html>.
- [22] NVIDIA Corporation. PhysicsNeMo: NVIDIA’s Open-Source Framework for Physics-Informed Machine Learning, 2023. URL <https://developer.nvidia.com/physicsnemo>. Formerly known as NVIDIA Modulus. Available as `nvidia-physicsnemo` on PyPI.